Purdue University
Purdue e-Pubs

Birck and NCN Publications | Birck Nanotechnology Center

8-2012

Thermal and Electrical Conductivities of Nanocrystalline Nickel Microbridges

Robert A. Sayer
Purdue University, Birck Nanotechnology Center, rsayer@purdue.edu

Juan Zeng
Purdue University, zengj@purdue.edu

Hao-Han Hsu
Purdue University, hsuh@purdue.edu

Dimitrios Peroulis
Purdue University, Birck Nanotechnology Center, dperouli@purdue.edu

Timothy S. Fisher
Purdue University, Birck Nanotechnology Center, tsfisher@purdue.edu

Follow this and additional works at: http://docs.lib.purdue.edu/nanopub

Part of the Nanoscience and Nanotechnology Commons

Sayer, Robert A.; Zeng, Juan; Hsu, Hao-Han; Peroulis, Dimitrios; and Fisher, Timothy S., "Thermal and Electrical Conductivities of Nanocrystalline Nickel Microbridges" (2012). *Birck and NCN Publications.* Paper 878.
http://dx.doi.org/10.1109/JMEMS.2012.2191938

This document has been made available through Purdue e-Pubs, a service of the Purdue University Libraries. Please contact epubs@purdue.edu for additional information.

Thermal and Electrical Conductivities of Nanocrystalline Nickel Microbridges

Robert A. Sayer, Juan Zeng, Hao-Han Hsu, Dimitrios Peroulis, *Member, IEEE*, and Timothy S. Fisher

***Abstract*—DC electrical self-heating (Joule heating) is exploited to characterize the thermal behavior of Ni microbridges. The temperature rise of the devices due to self-heating is monitored using an infrared microscope for current densities up to 10^5 A/cm^2. The obtained temperature profiles reveal significant heating at the bases of the microbridges. Simulations are performed in order to extract the thermal conductivity of the electroplated Ni thin film from the experimental data. The thermal conductivity is found to be 78.8 $\mathrm{W/m \cdot K}$ or 13% less than that of bulk Ni. As current flows through the microbridges, they deflect upward, significantly changing the system response and pull-in voltage required for actuation. Additionally, the electrical resistivity and specific electrical contact resistances between the microbridges and the anchor points are reported. The electroplated Ni is found to have an electrical resistivity of 9.7 $\mu\Omega \cdot$ cm which agrees with other values in the literature for thin-film Ni. By combining the electrical and thermal measurements, it is possible to determine the phonon and electron contributions to thermal conductivity. Although demonstrated on Ni films, this technique can be applied to any metallic film without modification. Such characterization of transport properties of constituent materials is important in the modeling of microelectromechanical systems and enables device performance to be predicted with improved accuracy. [2011-0295]**

***Index Terms*—Infrared (IR) imaging, microelectromechanical systems (MEMS), nickel, resistivity, self-heating, thermal conductivity.**

Manuscript received October 5, 2011; revised March 6, 2012; accepted March 15, 2012. Date of publication April 13, 2012; date of current version July 27, 2012. This work was supported in part by the National Nuclear Security Administration Center for Prediction of Reliability, Integrity, and Survivability of Microsystems, U.S. Department of Energy, under Award DE-FC52-08NA28617. Subject Editor D. L. DeVoe.

R. A. Sayer was with the School of Mechanical Engineering and the Birck Nanotechnology Center, Purdue University, West Lafayette, IN 47907 USA. He is now with Sandia National Laboratories, Albuquerque, NM 87185 USA (e-mail: rsayer@sandia.gov).

J. Zeng is with the School of Electrical and Computer Engineering and the Birck Nanotechnology Center, Purdue University, West Lafayette, IN 47907 USA.

H.-H. Hsu was with the School of Electrical and Computer Engineering and the Birck Nanotechnology Center, Purdue University, West Lafayette, IN 47907 USA. He is now with Intel Corporation, Hillsboro, OR 97124 USA.

D. Peroulis is with the School of Electrical and Computer Engineering, the School of Mechanical Engineering (by courtesy), and the Birck Nanotechnology Center, Purdue University, West Lafayette, IN 47907 USA (e-mail: dperouli@purdue.edu).

T. S. Fisher is with the School of Mechanical Engineering and the Birck Nanotechnology Center, Purdue University, West Lafayette, IN 47907 USA (e-mail: tsfisher@purdue.edu).

Color versions of one or more of the figures in this paper are available online at http://ieeexplore.ieee.org.

Digital Object Identifier 10.1109/JMEMS.2012.2191938

Nomenclature

A Area.
d Grain size.
dA Differential area.
dq Heat rate from differential area.
dx Differential length.
h Convective heat transfer coefficient.
h_{int} Thermal conductance of anchor.
g Acceleration due to gravity.
I Current.
$\mathbf{J}$ Flux.
k Thermal conductivity.
L Length.
P Perimeter.
Pr Prandtl number.
q Heat rate.
$\dot{q}$ Heat generation rate.
R Electrical resistance.
Ra Rayleigh number.
S Source term.
T Temperature.
t Thickness.
V Volume.
w Width.
x Distance.

Greek symbols
α Thermal diffusivity.
β Volumetric thermal expansion coefficient.
Δ Length of unit cell.
ε Emissivity.
ρ Resistivity.
σ Stefan–Boltzmann constant.
ν Kinematic viscosity.

Subscripts
C Constant.
c Cross section.
conv Convection.
f Film.
gen Generation.
rad Radiation.
nb Neighbor.
P Cell centroid value.
s Surface.
t Thickness.
w Width.
∞ Ambient.

Superscripts
$*$ Value from previous iteration.

1057-7157/$31.00 © 2012 IEEE

I. Introduction

THE SMALL length scales of microelectromechanical systems (MEMS) often lead to high current densities that can result in local temperature rises of hundreds of kelvins [1], [2]. In order to predict the thermal, mechanical, and electrical performance of microdevices, accurate material property information is essential. Although bulk thermal properties of materials are readily available in the literature, materials tend to exhibit different thermal properties when length scales are reduced to microscale dimensions because of boundary and/or microstructural effects [3]–[5]. This paper reports the electrical resistivity and thermal conductivity of a practical MEMS bridge element.

Electrical resistivity directly affects Joule heating of a material and therefore plays a critical role in thermal management of MEMS devices. Angadi and Udachan [6] measured the electrical resistivity of thermally evaporated Ni films ranging from 6 to 70 nm in thickness. The measured resistivity was strongly dependent on film thickness. A 20-nm-thick film exhibited a resistivity of 40 $\mu\Omega \cdot$ cm, which decreased to 19 $\mu\Omega \cdot$ cm for a 40-nm-thick film; both exceed the bulk value of 6.9 $\mu\Omega \cdot$ cm [7]. Similar trends were observed by Paddock and Eesley [8] for electron beam (e-beam)-evaporated and e-beam-sputtered Ni films. Johnson [9] investigated the effects of deposition conditions (deposition rate and substrate temperature) on the resistivity of thermally evaporated Ni. Increasing substrate temperature and deposition rate tended to result in decreased resistivity values. Aus *et al.* [10] measured the electrical resistivity of electroplated Ni films with average grain sizes ranging from 11 nm (20.6 $\mu\Omega \cdot$ cm) to 100 μm (7.4 $\mu\Omega \cdot$ cm). The observed trend of decreasing electrical resistivity with increasing grain size is attributed to the smaller volume fraction of interfaces associated with larger grains, and hence, boundary-related electron scattering events occur less frequently.

Reduced electrical conductivity at small scales leads to reduced thermal conductivity because the majority of heat flow in a metal is carried by electrons [11]. Early experimental work by Langer *et al.* [3] suggested that the thermal conductivity of thin-film Ni may not be reduced from bulk values. They measured films ranging in thickness from 0.4 to 8 μm and found that the thermal conductivity was around 90 W/m $\cdot$ K for all the films, which is in agreement with the bulk value of 90.7 W/m $\cdot$ K [12]. More recent experimental and theoretical works have suggested otherwise. Wang *et al.* [13] measured the thermal conductivity of a 1-μm-thick e-beam-evaporated Ni film to be 47.5 W/m $\cdot$ K using the photoacoustic technique, a value below that of bulk. Reduced thermal conductivity was also reported by Caffrey *et al.* [14], who used the transient thermoreflectance technique coupled with a pump–probe setup to measure thermal properties of thin metal films deposited on Si substrates. A 100-nm-thick Ni film, for example, was found to have a thermal conductivity of 52.7 W/m $\cdot$ K. Yuan and Jiang [15] investigated the effect of grain size on thermal conductivity of thin nickel films using nonequilibrium molecular dynamics. The computed room-temperature thermal conductivity of the films ranged from 67.8 to 79.9 W/m $\cdot$ K for grain sizes from 20 to 50 nm, respectively. Thermal conductivity values reduced below bulk values have also been reported in the literature for many other metals, including Ag [16], Al [17], Au [3], Cu [16], Pd [18], and Pt [14].

When a current is applied to a resistive device, self-heating, also known as Joule or resistive heating, will occur. Self-heating temperature profiles of MEMS devices are commonly measured using infrared (IR) thermography. For example, Reano *et al.* [19] measured the temperature rise of an RF MEMS capacitive switch in both the ON and OFF states for RF input powers up to 6.7 W. Although minimal temperature differences (< 7 K) were observed in the ON state, rises of up to 20 K were measured in the OFF state. Coccetti and Plana [20] used IR thermography to map the temperature profiles of both capacitive shunt and series RF MEMS switches. Temperature rises as large as 50 K were reported. Similar to the findings of Reano *et al.* [19], the measured temperature rise was greatest when the switch is OFF. Although IR thermography has been used to monitor self-heating in MEMS devices, these data have not been used to extract thermal properties or predict device performance.

In this paper, we present electrical and thermal measurements conducted on Ni microbridges [21] in order to extract material properties and predict the effect of self-heating on the switch's actuation voltage. Increased electrical resistivity and decreased thermal conductivity in comparison to bulk values are reported for the devices. DC electrical self-heating is monitored using IR thermography. The finite-volume method is then used to determine thermal conductivity by a fit to the measured temperature profiles. Additionally, microbridge deflection during self-heating is measured with a laser confocal microscope. Computer simulation [22] of the deflected profiles is performed to determine the change in actuation voltage of the switches due to self-heating.

II. Fabrication and Experiments

A. Device Fabrication

The Ni microbridges were fabricated on a p-type high-resistivity Si substrate with a 500-nm-thick thermally grown SiO_2 layer [23]. The fabrication procedure is shown in Fig. 1. First, a 1-μm-thick Au film is sputtered and lifted off to define the bottom electrodes and electrical connections of the microbridge, as shown in Fig. 1(a). The anchors are then patterned using a 3-μm-thick photoresist sacrificial layer [Fig. 1(b)]. The sacrificial layer is hard baked at 190 °C for 5 min. A seed layer of 50-nm sputtered Ti and 30-nm evaporated Ni is deposited on the whole sample, as shown in Fig. 1(c). Next, a 6-μm-thick photoresist layer is patterned to form the electroplating mold on the seed layer. The Ni electroplating is carried out in a nickel sulfamate bath at a temperature of 50 °C and a pH value of four. A 4-μm-thick Ni layer is selectively electroplated on the seed layer based on the photoresist mold, as shown in Fig. 1(d). After the removal of the photoresist mold, the Ni and Ti seed layers are stripped with 1:1 HCl:H_2O and 1:20 HF:H_2O at room temperature, respectively. The photoresist sacrificial layer is removed by immersion in photoresist stripper 2000 at 75 °C for 24 h. Finally, the fabrication process is completed by drying in a critical point dryer [Fig. 1(e)]. A scanning electron

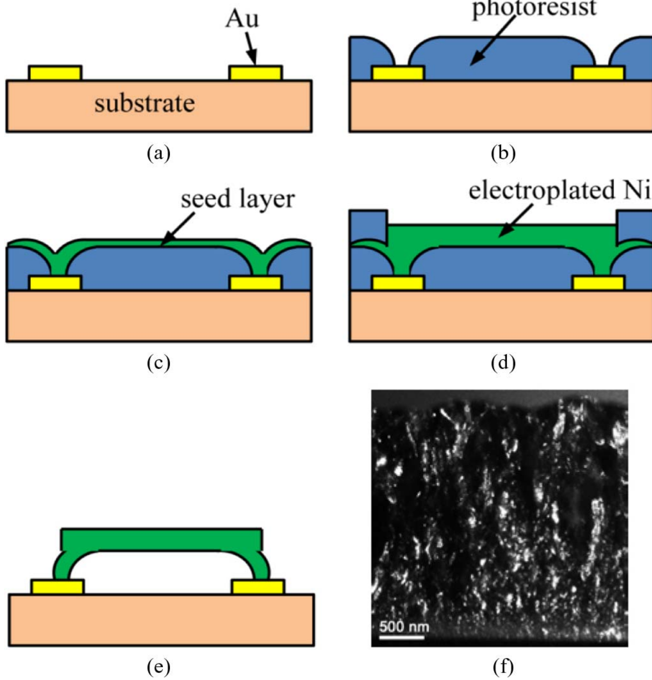

Fig. 1. (a)–(e) Fabrication process of the Ni RF MEMS microbridge. (f) Dark field TEM image of the Ni film (courtesy of P. R. Cantwell).

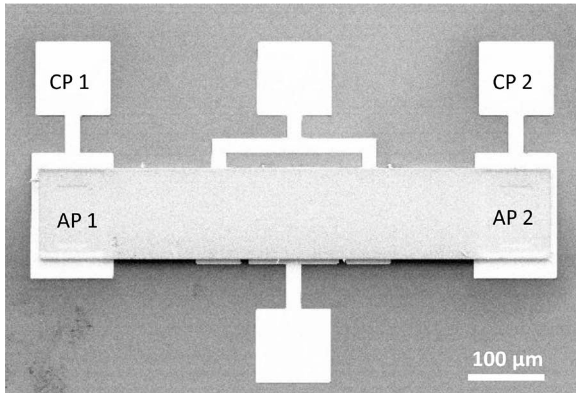

Fig. 2. SEM image of a microbridge. CP denotes a contact pad, and AP denotes an anchor point of the bridge to its support.

microscope (SEM) image of one of the microbridges is shown in Fig. 2.

The microstructure of the Ni was investigated using transmission electron microscopy (TEM). A dark field micrograph is shown in Fig. 1(f). The grain sizes are on the order of 10–50 nm with the majority of the crystals in the {001} and {111} orientations [23].

B. Experimental Setup

Electrical Characterization: The electrical resistivity of the Ni was measured using a four-probe measurement setup [24]. Current sourcing probes were connected to the contact pads (CPs) of the device (denoted by CP 1 and CP 2 in Fig. 2). Voltage sensing probes were placed on the top of the microbridge, one at each anchor point (AP) and spaced approximately 575 μm apart (as measured from center to center of the APs, the suspended length of the microbridges is 500 μm). This setup was used to eliminate the influence of contact resistance at the interface between the anchor and the microbridge that was found to be significant. The interfacial contact resistance between the anchor and the microbridge was also characterized using a four-probe measurement. For these measurements, current was sourced between the two CPs, and voltage was measured between the top of the microbridge directly above the AP and the nearest CP (i.e., between AP 1 and CP 1 in Fig. 2). The resistance of the metal leads is found to be negligible in comparison to the contact resistance, and therefore, the entire measured resistance is attributed to the interface.

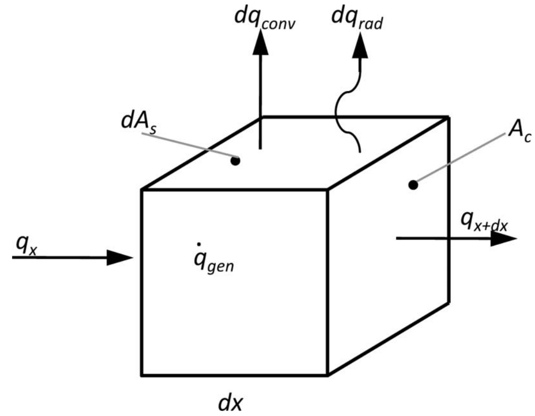

Fig. 3. Differential CV for 1-D conduction with radiation and free convection.

IR Thermography: IR thermography is a noninvasive temperature measurement technique that has been applied to MEMS [25]–[27], electronic components [26], [28], [29], and numerous other devices [30]–[32]. IR thermography operates on the principles of thermal radiation governed by the Stefan–Boltzmann law and can be used to make both steady and transient temperature measurements across a 3-D surface. This thermal imaging technique was employed to obtain 2-D temperature profiles of the Ni MEMS microbridges. Electrical probes are connected to the CPs (CP 1 and CP 2 in Fig. 2) of the device. A current source is used to pass dc currents ranging from 0 to 550 mA through the microbridge. An IR microscope with a spatial resolution of 2 μm and a temperature resolution of 0.3 K was used to measure the steady-state heating profiles.

Beam Deflection Measurements: As current flows through a microbridge, self-heating causes thermal expansion of the Ni, leading to thermal stresses that cause the microbridge to deflect from its original profile. A laser confocal microscope with horizontal and vertical resolutions of 0.6 and 0.1 μm, respectively, measures the vertical deflection of the microbridges. The experimental procedure is identical to that of the IR measurements, except that the IR microscope is replaced by a laser confocal microscope.

III. Thermal Analysis

The geometry of the microbridge can be represented thermally as a 1-D beam subjected to axial conduction, radiation, and free convection. Fig. 3 shows a control volume (CV)

representation of a differential cell. Performing an energy balance at steady state, the CV is governed by

$$q_x + \dot{q}_{\text{gen}} A_c dx = dq_{\text{conv}} + dq_{\text{rad}} + q_{x+dx} \tag{1}$$

where q_x and q_{x+dx} are the heat rates entering the CV at location x and leaving at location $x + dx$, respectively, and are given by

$$q_x = -\, kA_c \frac{dT}{dx} \tag{2}$$

$$q_{x+dx} = q_x + \frac{dq_x}{dx} dx \tag{3}$$

where k is the thermal conductivity, A_c is the cross-sectional area of the beam, and T is the temperature. x is the position along a beam of length L, where $x = 0$ corresponds to the center of the beam. $\dot{q}_{\text{gen}}$ is the volumetric heat generation in the CV due to Joule heating

$$\dot{q}_{\text{gen}} = \frac{I^2 R}{V} \tag{4}$$

where I is the current and R and V are the electrical resistance and volume of the beam, respectively. dq_{conv} and dq_{rad} are the heat losses due to convection and radiation, respectively, and are given by

$$dq_{\text{conv}} = h(T - T_\infty) dA_s \tag{5}$$

$$dq_{\text{rad}} = \varepsilon\sigma \left(T^4 - T_\infty^4\right) dA_s \tag{6}$$

where ε is the emissivity, σ is the Stefan–Boltzmann constant, h is the convective heat transfer coefficient, T_∞ is the ambient temperature, and dA_s is the surface area of the CV.

Substituting (2)–(6) into (1), the governing differential equation becomes

$$kA_c \frac{d^2T}{dx^2} + \frac{I^2 R}{L} - \varepsilon\sigma P \left(T^4 - T_\infty^4\right) - hP(T - T_\infty) = 0 \tag{7}$$

where P is the perimeter of the beam.

Equation (1) is commonly solved by assuming that the ends of the beam $(x = \pm L/2)$ exist at the ambient temperature [33], [34]. Sayer *et al.* [35] showed that, in a real device, the temperature at the beam ends can be elevated significantly above that of the ambient due to the finite thermal and electrical conductivities of the anchor. As a result, the following boundary condition is applied:

$$-k \left.\frac{dT}{dx}\right|_{x=\pm L/2} = h_{\text{int}}(T - T_\infty) \tag{8}$$

where h_{int} is the thermal conductance of the anchor.

Additionally, a symmetry (adiabatic) boundary condition can be applied to the center of the beam such that

$$\left.\frac{dT}{dx}\right|_{x=0} = 0. \tag{9}$$

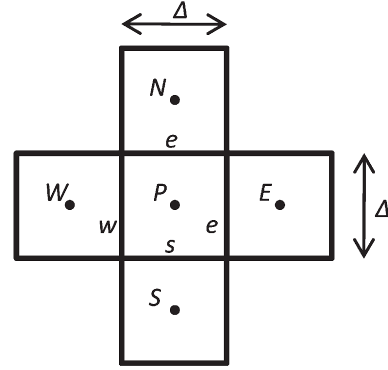

Fig. 4. Typical interior cell and its neighbors for a uniform structured mesh.

IV. Finite-Volume Method

The finite-volume method was used to solve the temperature profile of (7) numerically. The domain was discretized into a uniform structured grid [36]. Fig. 4(a) shows a typical interior cell P surrounded by its east, west, north, and south neighbors (denoted by E, W, N, and S, respectively). Consider the steady diffusion problem with a source term S

$$\nabla \cdot \mathbf{J} = S \tag{10}$$

where the flux $\mathbf{J}$ is

$$\mathbf{J} = -k\nabla T. \tag{11}$$

By integrating over the CV, applying the divergence theorem, and linearizing the source term $S = S_C + S_P T_P$, we find

$$\sum_{nb} \mathbf{J}_{nb} \cdot \mathbf{A}_{nb} = (S_C + S_P T_P)V \tag{12}$$

where V is the cell volume and the subscript nb denotes the neighbor faces (e, w, n, and s). The microbridge geometry can be simplified to a 1-D problem. By conducting an energy balance as described in (7), Joule heat generation, convection, and radiation are accounted for in the source term such that

$$S = \frac{I^2 R}{V} + \frac{\varepsilon\sigma P \left(T^4 - T_\infty^4\right) + hP(T - T_\infty)}{A_c} \tag{13}$$

$$S_C = S^* + \frac{4\varepsilon\sigma P {T^*}^4 + hPT^*}{A_c} \tag{14}$$

$$S_P = \frac{-\left(4\varepsilon\sigma {T^*}^3 + hP\right)}{A_c} \tag{15}$$

where the superscript $*$ represents values from the previous iteration.

V. Results

The electrical resistivity of the electroplated Ni microbridges was found to be $9.7 \pm 0.3\ \mu\Omega \cdot \text{cm}$. This value is 38% greater than that of bulk Ni and is compared to other thin-film values reported in the literature in Table I. Aus *et al.* [10] found that the electrical resistivity depends on the film thickness. Thinner films have higher resistivity in comparison to a thicker film due to the increased volume interfaces at smaller grain sizes

TABLE I
ELECTRICAL PROPERTIES OF THIN-FILM Ni

Property	Description	Value	Source
Resistivity ($\mu\Omega\cdot$cm)	Electroplated, 4 μm	9.7 ± 0.3	This work
	Electroplated, 100 μm	7.4	Ref. [10]
	Electroplated, 500 nm	10.5	Ref. [10]
	Electroplated, 34 nm	15.6	Ref. [10]
	Electroplated, 15 nm	20.3	Ref. [10]
	Electroplated, 11 nm	20.6	Ref. [10]
	Thermal evap., 1 μm	12.0	Ref. [9]
	e-beam evap., 450 nm	11.2	Ref. [8]
	Sputtered, 60 nm	17.8	Ref. [8]
	Thermal evap., 40 nm	19.0	Ref. [6]
	Thermal evap., 20 nm	40.0	Ref. [6]
	Nanowire, 100 nm	34.0	Ref. [5]
	Bulk	6.9	Ref. [7]
Specific contact resistance ($\mu\Omega\cdot cm^2$)	Electroplated, 4 μm	56 ± 39	This work

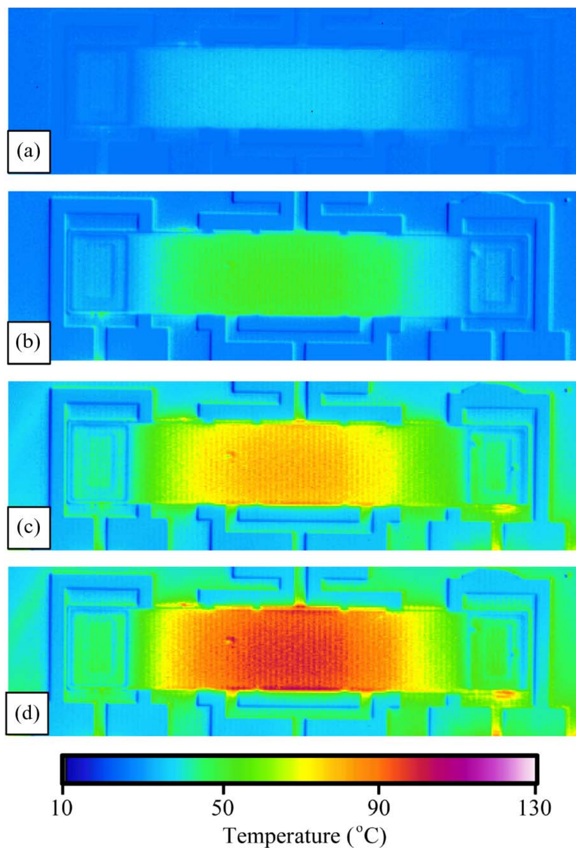

Fig. 5. IR thermograms of a typical Ni microbridge for currents of (a) 300 mA, (b) 400 mA, (c) 500 mA, and (d) 550 mA.

and the associated increased electron scattering at the grain boundaries. The electrical contact resistance between the beam and the anchor was found to be $1.7 \pm 1.2\ \Omega$, which corresponds to a specific contact resistance of 56 $\mu\Omega \cdot \mathrm{cm}^2$.

The self-heating of several devices was measured in air at an ambient temperature of 296 K. The temperature profile of a typical beam under heating conditions up to 550 mA is shown in the thermograms in Fig. 5. The temperature profile is symmetric about the middle of the beam ($x = 0$) and was confirmed to be independent of electrical polarity. Additionally, the temperature

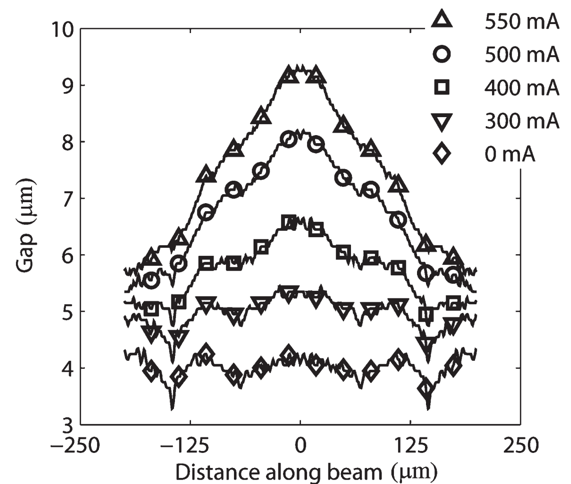

Fig. 6. Centerline temperature profiles averaged over all tested microbridges.

across the width of the beam is essentially uniform for all x locations along the beam. The horizontal centerline temperature profile averaged over all tested devices is shown in Fig. 6. The temperature of the microbridge increases along the entire length as the applied current increases. A maximum temperature rise of approximately 75 K is observed for an applied current of 550 mA. Significant heating can also be observed in the anchor of the device. The temperature rise at the base of the microbridge is approximately 30% of the maximum temperature rise in the beam for all applied currents. The heating of the beam anchors is attributed to the thermal resistance of the anchors.

The temperature profiles on the Ni microbridge described by (12) were determined using the finite-volume method. The dimensions of the microbridge were obtained from SEM images of the devices. The emissivity of Ni was measured to be 0.09, which is in good agreement with that in the literature [37], [38], and the heat transfer coefficient was calculated according to Bejan [39]. Ni thermal conductivity and the thermal resistance of the anchor were treated as fitting parameters. Due to the large change in temperature across the device (75 K at 550 mA), thermal conductivity cannot be assumed constant. Rather, it was assumed to decrease linearly with temperature over the range of interest [40]. The fitted parameters were selected from the combination that yielded the smallest residual sum of squares between the experimental and numerical temperature profiles. The thermal resistance of the anchor was found to be $1.3 \times 10^6\ \mathrm{W/m^2 \cdot K}$. This value is in good agreement with experimental observations of temperature rise at the beam ends and was taken as a known parameter in all subsequent analysis.

The thermal conductivity of the Ni at 300 K is found to be $78.8 \pm 1.2\ \mathrm{W/m \cdot K}$, where the uncertainty is found using bootstrapping [41], [42]. Table II compares this value to others for thin films and bulk reported in the literature. The measured thermal conductivity is 13% below that of bulk Ni and in good agreement with the theoretical value of 79.9 $\mathrm{W/m \cdot K}$ for a film with a grain size of 50 nm [15]. The temperature profiles calculated using the finite-volume method for Ni thermal conductivity values of 67, 78.8 (measured value), and 90.7 (bulk value) $\mathrm{W/m \cdot K}$ are compared to the experimental results in

TABLE II
THERMAL PROPERTIES OF THIN-FILM Ni

Property	Description	Value	Source
Thermal conductivity (W/mK)	Electroplated, 4 µm	78.8 ± 1.2	This work
	e-beam evap., 1 µm	47.5	Ref. [13]
	e-beam evap., 100 nm	52.7	Ref. [14]
	NEMD, 50 nm	79.9	Ref. [15]
	0.4-8 µm	90.0	Ref. [3]
	Bulk	90.7	Ref. [12]

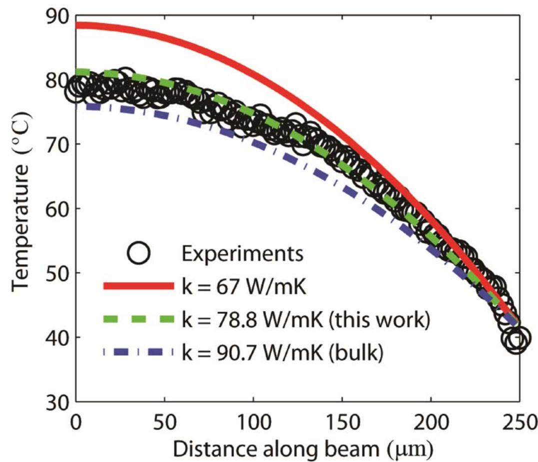

Fig. 7. Calculated microbridge temperature profiles for Ni thermal conductivity values of 67, 78.8, and 90.7 $\mathrm{W/m \cdot K}$ compared to the experimental results for an input current of 550 mA.

Fig. 7. It is evident that the middle curve accurately fits to the data while the other two values (67 and 91 $\mathrm{W/m \cdot K}$) predict temperature profiles that are too high or too low, respectively.

A simple Wiedemann–Franz analysis [43] using the measured electrical resistivity reveals an extracted electronic thermal conductivity of 74.6 $\mathrm{W/m \cdot K}$ at room temperature, which is in close agreement with our thermal measurement. The slightly higher measured thermal conductivity results from the contribution of phonons to thermal conduction which is not captured by the Wiedemann–Franz analysis. The phonon contribution of 4.2 $\mathrm{W/m \cdot K}$ is about 40% less than that of bulk Ni [44]. If electrical resistivity was used to calculate thermal conductivity instead of the IR temperature profiles, we would underpredict the value by about 5%. The error would be greater in materials where phonon conduction comprises a larger fraction of the total thermal conductivity. This illustrates the importance of using nonelectrical-resistance-based measurements for determining thermal properties. More importantly, by combining the Wiedemann–Franz analysis with the IR measurements, it is possible to measure the electronic and phononic contributions to thermal conductivity individually.

Wang [45] determined an empirical relationship of thermal conductivity as a function of grain size for nanocrystalline Ni films

$$k = \left(86.5 - 2.20 \times 10^{-7} \frac{2.37}{d}\right) \left[\frac{\mathrm{W}}{\mathrm{m \cdot K}}\right] \quad (16)$$

where d is the grain size in meters, 2.20×10^{-7} is the specific grain boundary thermal resistance in units of watts per kelvin, and the term $2.37/d$ represents the grain boundary surface area per unit volume. This relation yields an average grain size of the tested Ni films to be 67 nm, which is in good agreement with that observed under TEM. It is noteworthy that the Ni films measured by Wang [45] were nominally 1 mm thick and the microbridges of this study were 4 μm in thickness. Although the thickness between the samples in the two studies varies by two to three orders of magnitude, both films follow the same empirical relationship. As a result, the reduction in thermal conductivity compared to the bulk value is not a surface scattering phenomenon; rather, it is solely due to grain boundary scattering.

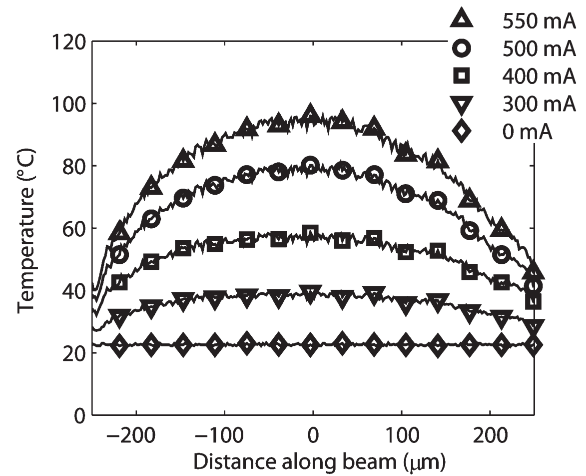

Fig. 8. Centerline height profiles averaged over all tested microbridges. Data at the edge of the beam have been omitted due to light scattering.

Self-heating during operation will cause thermal expansion of the Ni film. The APs of the microbridge resist the expansion of the film, thus giving rise to thermal compressive stress that causes the beam to deform in the vertical direction. As the microbridge deforms, the gap between the suspended film and the actuation electrodes increases. The average centerline profile of the microbridges is shown in Fig. 8 for heating currents ranging from 0 to 550 mA. Initially, the beam is not perfectly flat, but rather, it is slightly curved. As the heating current increases, the beam deflects upward, increasing the overall gap between the microbridge and substrate. Under maximum heating, the center of the beam ($x = 0$) deforms 5.3 μm upward, more than doubling the initial gap. We note that the measured beam deflection is on the order expected, as calculated using a simplified Euler–Bernoulli analysis [46]. The increased gap height can have a profound effect on the pull-in voltage required to actuate the switch in the ON state.

A 2-D beam model that incorporates residual stress, nonlinear stretching, platelike bending, squeeze film damping, electrostatic force, and beam/substrate impact developed by Snow and Bajaj [22] was used to predict the pull-in voltage required to actuate the switch to the ON state for three different Ni thermal conductivity values [47.5 $\mathrm{W/m \cdot K}$ [13], 78.8 $\mathrm{W/m \cdot K}$ (this work), and 90.7 $\mathrm{W/m \cdot K}$ (bulk)]. Fig. 9 shows the predicted pull-in voltages for the beam. For the zero heating case ($I = 0$ mA), 160 V is required to actuate the switch. A significant increase in actuation voltage is computed as the heating current in the microbridge is increased. At the

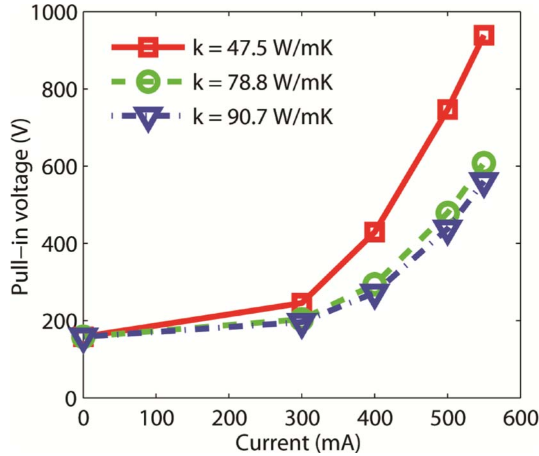

Fig. 9. Simulated pull-in voltages of the Ni MEMS switches under dc heating for Ni thermal conductivity values of 47.5, 78.8, and 90.7 $\mathrm{W/m \cdot K}$.

maximum applied current of 550 mA, the pull-in voltage is 610 V, a nearly fourfold increase from the unheated microbridge. Under dc heating, the pull-in voltage of the tested Ni switch is about 10% greater than what would be expected of a beam exhibiting bulk thermal properties. If the thermal conductivity is reduced to that reported in [13], the pull-in voltage increases by more than 50%. These results show that self-heating must be accounted for in the design process to ensure proper operation of electrostatically actuated MEMS switches.

VI. Conclusion

Self-heating arising from the finite thermal and electrical conductivities of materials and deformation due to thermal expansion under self-heating conditions are two important factors that must be considered in the design of microscale devices. In this paper, dc electrical self-heating in Ni microbridges has been monitored using IR thermography. The obtained heating profiles were used in combination with the finite-volume method to determine the thermal conductivity of the 4-μm-thick film with grain sizes ranging from 10 to 50 nm. The resulting thermal conductivity was found to be 78.8 $\mathrm{W/m \cdot K}$. Additionally, the electrical resistivity of the Ni film was measured to be 9.7 $\mu\Omega \cdot \mathrm{cm}$ using a four-probe setup. By using a Wiedemann–Franz analysis in combination with the IR testing, it is possible to measure both the electronic and phononic contributions to thermal conductivity. Additionally, self-heating of the microbridge caused the center of the beam to deflect 5.3 μm upward under maximum heating conditions, leading to a fourfold increase in the predicted actuation of the switch. Knowledge of these thin-film transport properties enables thermal management to be accounted for in the design of MEMS devices, thus permitting one to predict device performance with better accuracy.

Appendix A
Calculation of Heat Transfer Coefficient

Consider a thin cross-sectional slice of width Δ at any location x along the microbridge. The surface of the slice can be divided into four sections: two vertical and two horizontal walls all held at a constant temperature. For the vertical surface, we have [47]

$$h = \frac{k}{t}\left\{0.68 + \frac{0.67Ra_t^{1/4}}{\left[1+(0.49/Pr)^{9/16}\right]^{4/9}}\right\} \tag{A.1}$$

where k is the thermal conductivity of air, t is the thickness of the beam, Pr is the Prandtl number of air, and Ra is the Rayleigh number given by

$$Ra_t = \frac{g\beta(T-T_\infty)t^3}{\nu\alpha} \tag{A.2}$$

where g is the acceleration due to gravity, β is the volumetric thermal expansion coefficient, and α and ν are the thermal diffusivity and kinematic viscosity of air, respectively. All fluid properties are evaluated at the film temperature $T_f = 0.5\,(T + T_\infty)$.

For the upper horizontal surface, the heat transfer coefficient is given by [48]

$$h = \frac{0.54k \cdot Ra_w^{\frac{1}{4}}}{w} \tag{A.3}$$

where w is the width of the beam and

$$Ra_w = \frac{g\beta(T-T_\infty)w^3}{\nu\alpha}. \tag{A.4}$$

For the lower horizontal surface, the heat transfer coefficient is given by [39]

$$h = \frac{0.27k \cdot Ra_w^{1/4}}{w}. \tag{A.5}$$

Acknowledgment

The authors would like to thank the Air Force Research Laboratory Thermal Materials and Manufacturing Branch (RXBT) for use of the infrared microscope.

References

[1] H. T. Lim, F. Udrea, D. M. Garner, and W. I. Milne, "Modelling of self-heating effect in thin SOI and partial SOI LDMOS power devices," *Solid-State Electron.*, vol. 43, no. 7, pp. 1267–1280, Jul. 1999.

[2] R. A. Sayer, S. Kim, A. D. Franklin, S. Mohammadi, and T. S. Fisher, "Shot noise thermometry for thermal characterization of templated carbon nanotubes," *IEEE Trans. Compon. Packag. Technol.*, vol. 33, no. 1, pp. 178–183, Mar. 2010.

[3] G. Langer, J. Hartmann, and M. Reichling, "Thermal conductivity of thin metallic films measured by photothermal profile analysis," *Rev. Sci. Instrum.*, vol. 68, no. 3, pp. 1510–1513, Mar. 1997.

[4] A. D. McConnell, S. Uma, and K. E. Goodson, "Thermal conductivity of doped polysilicon layers," *J. Microelectromech. Syst.*, vol. 10, no. 3, pp. 360–369, Sep. 2001.

[5] M. N. Ou, S. R. Harutyunyan, S. J. Lai, C. D. Chen, T. J. Yang, and Y. Y. Chen, "Thermal and electrical transport properties of a single nickel nanowire," *Phys. Stat. Sol. B, Basic Solid State Phys.*, vol. 244, no. 12, pp. 4512–4517, Dec. 2007.

[6] M. A. Angadi and L. A. Udachan, "Electrical-properties of thin nickel films," *Thin Solid Films*, vol. 79, no. 2, pp. 149–153, May 1981.

[7] E. A. Belskaya and V. E. Peletskii, "Electrical resistivity of nickel in the temperature range 100–1700 degrees K," *High Temp.*, vol. 19, pp. 375–381, 1981.

[8] C. A. Paddock and G. L. Eesley, “Transient thermoreflectance from thin metal films,” *J. Appl. Phys.*, vol. 60, no. 1, pp. 285–290, Jul. 1986.

[9] B. C. Johnson, “Electrical resistivity of copper and nickel thin-film interconnections,” *J. Appl. Phys.*, vol. 67, no. 6, pp. 3018–3024, Mar. 1990.

[10] M. J. Aus, B. Szpunar, U. Erb, A. M. Elsherik, G. Palumbo, and K. T. Aust, “Electrical resistivity of bulk nanocrystalline nickel,” *J. Appl. Phys.*, vol. 75, no. 7, pp. 3632–3634, Apr. 1994.

[11] S. Kumar and G. C. Vradis, “Thermal conductivity of thin metallic films,” *J. Heat Transf.*, vol. 116, no. 1, pp. 28–34, Feb. 1994.

[12] F. P. Incropera and D. P. DeWitt, *Introduction to Heat Transfer*. New York: Wiley, 2002.

[13] X. Wang, H. Hu, and X. Xu, “Photo-acoustic measurement of thermal conductivity of thin films and bulk materials,” *J. Heat Transf.*, vol. 123, no. 1, pp. 138–144, Feb. 2001.

[14] A. P. Caffrey, P. E. Hopkins, J. M. Klopf, and P. M. Norris, “Thin film non-noble transition metal thermophysical properties,” *Microscale Thermophys. Eng.*, vol. 9, no. 4, pp. 365–377, Dec. 2005.

[15] S. P. Yuan and P. X. Jiang, “Thermal conductivity of nanoscale thin nickel films,” *Progr. Nat. Sci.*, vol. 15, no. 10, pp. 922–929, Oct. 2005.

[16] S. Ryu, W. Juhng, and Y. Kim, “Effect of microstructure on thermal conductivity of Cu, Ag thin films,” *J. Nanosci. Nanotechnol.*, vol. 10, no. 5, pp. 3406–3411, May 2010.

[17] N. Stojanovic, Y. Jongsin, E. B. K. Washington, J. M. Berg, M. W. Holtz, and H. Temkin, “Thin-film thermal conductivity measurement using microelectrothermal test structures and finite-element-model-based data analysis,” *J. Microelectromech. Syst.*, vol. 16, no. 5, pp. 1269–1275, Oct. 2007.

[18] A. Yarai and T. Nakanishi, “In-situ thermoproperties measurement of Pd film deposited onto optical fiber prepared for photothermal reflectance detection,” *J. Phys., Conf. Ser.*, vol. 214, no. 1, p. 012 055, 2010.

[19] R. M. Reano, D. Peroulis, J. F. Whitaker, and L. P. B. Katehi, “Electro/thermal measurements of RF MEMS capacitive switches,” in *IEEE MTT-S Int. Microw. Symp. Dig.*, 2003, pp. 1923–1926.

[20] F. Coccetti and R. Plana, “Simultaneous electro-thermal experimental analysis of RF-MEMS switches for high microwave power handling,” *Phys. Stat. Sol. (A)*, vol. 205, no. 11, pp. 2647–2650, Nov. 2008.

[21] A. K. Mahapatro, J. Chee, and D. Peroulis, “Fully electronic method for quantifying the post-release gap-height uncertainty of capacitive RF MEMS switches,” in *Proc. IEEE MTT*, 2009, pp. 1645–1648.

[22] M. G. Snow and A. K. Bajaj, “Comprehensive reduced-order models of electrostatically actuated MEMS switches and their dynamics including impact and bounce,” in *Proc. ASME Conf.*, 2010, vol. 2010, pp. 579–588.

[23] P. R. Cantwell, H. Kim, M. M. Schneider, H.-H. Hsu, D. Peroulis, E. A. Stach, and A. Strachan, *Estimating the in-plane Young's modulus of polycrystalline films in MEMS*, [Online]. Available: http://ieeexplore.ieee.org, DOI: 1.1109/JMEMS.2012.2191939.

[24] W. Boley, T. Bhuvana, B. Hines, R. A. Sayer, G. Chiu, T. S. Fisher, D. Bergstrom, R. Reifenberger, and G. U. Kulkarni, “Inkjet printing involving palladium alkanethiolates and carbon nanotubes functionalized with single-strand DNA,” in *Proc. NIP 25—Digital Fabrication, Tech. Program*, Louisville, KY, 2009, pp. 824–827.

[25] P. Fürjes, G. Bognár, and I. Bársony, “Powerful tools for thermal characterisation of MEMS,” *Sens. Actuators B, Chem.*, vol. 120, no. 1, pp. 270–277, Dec. 2006.

[26] R. H. Hopper, C. H. Oxley, J. W. Pomeroy, and M. Kuball, “Micro-Raman/infrared temperature monitoring of Gunn diodes,” *IEEE Trans. Electron Devices*, vol. 55, no. 4, pp. 1090–1093, Apr. 2008.

[27] B. Serio, J. J. Hunsinger, F. Conseil, P. Derderian, D. Collard, L. Buchaillot, and M. F. Ravat, “Close infrared thermography using an intensified CCD camera: Application in nondestructive high resolution evaluation of electrothermally actuated MEMS,” in *Proc. Opt. Meas. Syst. Ind. Inspection IV, Pts. 1 and 2*, W. Osten, C. Gorecki, and E. Novak, Ed.s, 2005, vol. 5856, pp. 819–829.

[28] S. Dhokkar, B. Serio, P. Lagonotte, and P. Meyrueis, “Power transistor near-infrared microthermography using an intensified CCD camera and frame integration,” *Meas. Sci. Technol.*, vol. 18, no. 8, pp. 2696–2703, Aug. 2007.

[29] R. Grimes and M. Davies, “Optical measurement of electronic system air flow and temperature distribution,” *J. Opt. A, Pure Appl. Opt.*, vol. 6, no. 6, pp. 617–626, Jun. 2004.

[30] D. B. Go, R. A. Maturana, T. S. Fisher, and S. V. Garimella, “Enhancement of external forced convection by ionic wind,” *Int. J. Heat Mass Transf.*, vol. 51, no. 25/26, pp. 6047–6053, Dec. 2008.

[31] X. J. Hu, M. A. Panzer, and K. E. Goodson, “Infrared microscopy thermal characterization of opposing carbon nanotube arrays,” *J. Heat Transf.*, vol. 129, no. 1, pp. 91–93, Jan. 2007.

[32] T. Westover, T. S. Fisher, and F. Pfefferkorn, “Experimental characterization of anode heating by electron emission from a multi-walled carbon nanotube,” *Int. J. Heat Mass Transf.*, vol. 50, no. 3/4, pp. 595–604, Feb. 2007.

[33] S. Shojaei-Zadeh, Z. Shu, L. Wenjun, Y. Yizhang, S. M. Sadeghipour, M. Asheghi, and P. Sverdrup, “Thermal characterization of thin film Cu interconnects for the next generation of microelectronic devices,” in *Proc. 9th Intersoc. Conf. Therm. Thermomech. Phenom. Electron. Syst.*, 2004, vol. 2, pp. 575–583.

[34] Y. C. Tai, C. H. Mastrangelo, and R. S. Muller, “Thermal conductivity of heavily doped low-pressure chemical vapor deposited polycrystalline silicon films,” *J. Appl. Phys.*, vol. 63, no. 5, pp. 1442–1447, Mar. 1988.

[35] R. A. Sayer, E. S. Piekos, and L. M. Phinney, “Modified data analysis for thermal conductivity measurements of polycrystalline silicon microbridges using a steady state Joule heating technique,” in *Proc. PRISM Seminar Ser.*, 2009.

[36] J. Y. Murthy, W. J. Minkowycz, E. M. Sparrow, and S. R. Mathur, “Survey of Numerical Methods,” in *Handbook of Numerical Heat Transfer*, 2nd ed, W. J. Minkowycz, E. M. Sparrow, and J. Y. Murthy, Eds. Hoboken, NJ: Wiley, 2006.

[37] B. T. Barnes, “Total radiation from polished and from soot-covered nickel,” *Phys. Rev.*, vol. 34, no. 7, pp. 1026–1030, Oct. 1929.

[38] M. F. Modest, *Radiative Heat Transfer*, 2nd ed. San Diego, CA: Academic, 2003.

[39] A. Bejan, *Convection Heat Transfer*, 2nd ed. New York: Wiley, 1995.

[40] C. Y. Ho, R. W. Powell, and P. E. Liley, “Thermal conductivity of the elements,” *J. Phys. Chem. Ref. Data*, vol. 1, no. 2, p. 279, Apr. 1972.

[41] B. Efron, “Bootstrap methods: Another look at the jackknife,” *Ann. Stat.*, vol. 7, no. 1, pp. 1–26, Jan. 1979.

[42] B. Efron and R. Tibshirani, “Statistical data analysis in the computer age,” *Science*, vol. 253, no. 5018, pp. 390–395, Jul. 12, 1991.

[43] N. W. Ashcroft and N. D. Mermin, *Solid State Physics*. New York: Saunders College, 1976.

[44] S. P. Yuan and P. X. Jiang, “Thermal conductivity of small nickel particles,” *Int. J. Thermophys.*, vol. 27, no. 2, pp. 581–595, Mar. 2006.

[45] S. Wang, “Thermal Conductivity of Nanocrystalline Nickel,” M.S. thesis, Mater. Sci. Eng., Univ. Toronto, Toronto, ON, Canada, 2011.

[46] J. M. Gere and B. J. Goodno, *Mechanics of Materials*, 7th ed. Toronto, ON, Canada: Cengage Learning, 2009.

[47] S. W. Churchill and H. H. S. Chu, “Correlating equations for laminar and turbulent free convection from a vertical plate,” *Int. J. Heat Mass Transf.*, vol. 18, no. 11, pp. 1323–1329, Nov. 1975.

[48] J. R. Lloyd and W. R. Moran, “Natural convection adjacent to horizontal surfaces of various planforms,” *J. Heat Transf.*, vol. 96, no. 4, pp. 443–451, Nov. 1974.

Robert A. Sayer received the B.S. degree in mechanical engineering from The Ohio State University, Columbus, in 2006, and the Ph.D. degree in mechanical engineering from Purdue University, West Lafayette, IN, in 2011.

He was a Member of the Nanoscale Transport Research Group, Purdue University, where his research focused on thermal property measurements and electrical shot noise measurements of micro-/nanoscale devices. He is currently a Senior Member of the Technical Staff with Sandia National Laboratories, Albuquerque, NM. His research interests include microscale and interfacial heat transfer, energy conversion, and applications and integration of carbon nanotubes into electrical systems.

Juan Zeng received the B.S. degree in microelectronic science and technology from Harbin Institute of Technology, Harbin, China, in 2007, and the M.S. degree in electrical and computer engineering from Tufts University, Medford, MA, in 2009. She is currently working toward the Ph.D. degree in electrical and computer engineering at Purdue University, West Lafayette, IN. Her current Ph.D. research focuses on device modeling and material property characterization of RF microelectromechanical systems devices.

Ms. Zeng was a recipient of the Dean's Fellowship in her Master's program and the Student Paper Award at the 2009 Midwest Symposium on Circuits and Systems.

Hao-Han Hsu received the B.S. and M.S. degrees in electrical engineering from National Tsing Hua University, Hsinchu, Taiwan, in 2001 and 2002, respectively, and the Ph.D. degree from the School of Electrical and Computer Engineering, Purdue University, West Lafayette, IN, in 2011. His doctoral research focused on reliability of RF microelectromechanical systems devices.

He is currently an Electromagnetic Compatibility Engineer with Intel Corporation, Hillsboro, OR.

Mr. Hsu was the recipient of the Student Paper Award at the 2011 IEEE Topical Meeting on Silicon Monolithic Integrated Circuits in RF Systems.

Dimitrios Peroulis (S'99–M'04) received the Ph.D. degree in electrical engineering from the University of Michigan, Ann Arbor, in 2003.

Since August 2003, he has been with Purdue University, West Lafayette, IN, where he is currently leading a group of graduate students on a variety of research projects in the areas of RF microelectromechanical systems (MEMS), sensing and power harvesting applications, and RF identification sensors for the health monitoring of sensitive equipment. He has been the Principal Investigator (PI) or a co-PI in numerous projects funded by government agencies and industry in these areas. He is currently a Key Contributor in two Defense Advanced Research Projects Agency (DARPA) projects at Purdue University focusing on the following: 1) very high quality ($Q > 1000$) RF tunable filters in mobile form factors (DARPA Analog Spectral Processing Program Phases I, II, and III) and 2) developing comprehensive characterization methods and models for understanding the viscoelasticity/creep phenomena in high-power RF MEMS devices (DARPA NEMS/MEMS Science and Technology Fundamentals Program Phases I and II). Furthermore, he is leading the experimental program in the Center for Prediction of Reliability, Integrity and Survivability of Microsystems funded by the National Nuclear Security Administration. In addition, he led the development of the MEMS technology in a U.S. Navy project (Marines) funded under the Technology Insertion Program for Savings program focused on harsh-environment wireless microsensors for the health monitoring of aircraft engines. He has over 170 refereed journal and conference publications in the areas of microwave integrated circuits, sensors, and antennas.

Dr. Peroulis was a recipient of a National Science Foundation CAREER Award in 2008. His students have received numerous student paper awards and other student research-based scholarships. He is recognized as a Purdue University Faculty Scholar and was also a recipient of ten teaching awards, including the 2010 HKN C. Holmes MacDonald Outstanding Teaching Award and the 2010 Charles B. Murphy Award, which is Purdue University's highest undergraduate teaching honor.

Timothy S. Fisher received the B.S. and Ph.D. degrees in mechanical engineering from Cornell University, Ithaca, NY, in 1991 and 1998, respectively.

Prior to his graduate studies, from 1991 to 1993, he was a Design Engineer with the Automotive and Industrial Electronics Group, Motorola, Inc. For several years, he was with Vanderbilt University, Nashville, TN. Since 2002, he has been with the School of Mechanical Engineering and the Birck Nanotechnology Center, Purdue University, West Lafayette, IN. His research has included efforts in simulation and measurement of nanoscale heat transfer, coupled electrothermal effects in semiconductor devices, nanoscale direct energy conversion, molecular electronics, microfluidic devices, hydrogen storage, and computational methods ranging from atomistic to continuum scales. Applications of his work cover a broad range of areas, including nanoelectronics, thermal interface materials, thermal–electrical energy conversion, biosensors, and hydrogen storage.

Dr. Fisher serves on the IEEE TC-9 Committee on Thermal Phenomena in Electronics, the American Society of Mechanical Engineers (ASME) K-6 Committee on Heat Transfer in Energy Systems, and the ASME K-16 Committee on Thermal Management of Electronics. He is a member of the Tau Beta Pi and Pi Tau Sigma honor societies.